Extent, heritability, and functional relevance of single cell expression variability in highly homogeneous populations of human cells

Daniel Osorio[1,#], Xue Yu[2,#], Yan Zhong[3,#], Guanxun Li[3], Peng Yu[4], Erchin Serpedin[4], Jianhua Huang[3,*], James J. Cai[1,4,5,*]

[1]Department of Veterinary Integrative Biosciences; [2]Department of Veterinary Pathobiology; [3]Department of Statistics; [4]Department of Electrical and Computer Engineering; [5]Interdisciplinary Program of Genetics; Texas A&M University, College Station, TX 77843, USA.

[#]These authors contributed equally to this work.

[*]Corresponding authors: JH (jianhua@stat.tamu.edu) and JJC (jcai@tamu.edu)

Keywords: single-cell RNA sequencing, scRNA-seq, single cell expression variability, cell-to-cell variation, lymphoblastoid cell line, airway epithelial cell, dermal fibroblast

Alternative title: Single cell expression variability in highly homogeneous populations of human cells is widespread, heritable, and implies cell function

Abstract

Because of recent technological developments, single-cell assays such as single-cell RNA sequencing (scRNA-seq) have become much more widely available and have achieved unprecedented resolution in revealing cell heterogeneity. The extent of intrinsic cell-to-cell variability in gene expression, or *single cell expression variability* (scEV), has thus been increasingly appreciated. However, it remains unclear whether this variability is functionally important and, if so, what its implications are for multi-cellular organisms. We therefore analyzed multiple scRNA-seq data sets from lymphoblastoid cell lines (LCLs), lung airway epithelial cells (LAECs), and dermal fibroblasts (DFs). For each of the three cell types, we estimated scEV in homogeneous populations of cells; we identified 465, 466, and 291 highly variable genes (HVGs), respectively. These HVGs were enriched with specific functions precisely relevant to the cell types, from which the scRNA-seq data used to identify HVGs were generated—e.g., HVGs identified in lymphoblastoid cells were enriched in cytokine signaling pathways, LAECs collagen formation, and DFs keratinization. HVGs were deeply embedded in gene regulatory networks specific to corresponding cell types. We also found that scEV is a heritable trait, partially determined by cell donors' genetic makeups. Furthermore, across genes, especially immune genes, levels of scEV and between-individual variability in gene expression were positively correlated, suggesting a potential link between the two variabilities measured at different organizational levels. Taken together, our results support the "variation is function" hypothesis, which postulates that scEV is required for higher-level system function. Thus, we argue that quantifying and characterizing scEV in relevant cell types may deepen our understating of normal as well as pathological cellular processes.

Introduction

Cells are fundamental units of cellular function. Cells in multi-cellular organisms can be organized into groups, or cell types, based on shared features that are quantifiable. A multicellular organism is usually composed of cells of many different types—each is a distinct functional entity differing from the other. Within the same cell type, cells are nearly identical and are considered to carry the same function.

The recent development of single cell RNA sequencing (scRNA-seq) technologies has brought the increasingly high-resolution measurements of gene expression in single cells (Zhang et al. 2019). This power has been widely adopted to refine the categories of known cell types and analyze complex tissues systematically and reproducibly (Buettner et al. 2015). The power of scRNA-seq has also been harnessed to identify novel cellular states among the same type of cells (Trapnell 2015).

Cells of the same type and the same state may still show marked intrinsic cell-to-cell variability in gene expression or *single cell expression variability* (scEV), even under the same environmental conditions (Ko 1992; Fiering et al. 2000; Raj and van Oudenaarden 2008). The importance of this intrinsic variability is increasingly appreciated (Eldar and Elowitz 2010; Pelkmans 2012). Changes in the magnitude of scEV have been associated with development (Wernet et al. 2006; Chang et al. 2008; Faure et al. 2017; Kumar et al. 2017), aging (Martinez-Jimenez et al. 2017; Wiley et al. 2017), and pathological processes (Segerstolpe et al. 2016; Azizi et al. 2018).

Dueck and colleagues (Dueck et al. 2016) put forward the so-called "variation is function" hypothesis, saying that scEV *per se* might be crucial for population-level function. They used the term "single cell variation or variability" to refer to diversity within an ensemble that has been previously defined as being generally homogeneous, rather than diversity of cell types that are clearly distinct and already recognized. The main focus of their question is to ask how the individual cells with different gene expression levels may interact to causally generate higher-level function. If the hypothesis turns out to be true, it means that the intrinsic cell-to-cell variability is an indicator of a diversity of hidden functional capacities, which facilitate the collective behavior of cells. This collective behavior is essential for the function and normal development of cells and tissues (Raj et al. 2010; Tay et al. 2010). The loss of this collective cellular behavior may result in disease. Thus, investigation of the intrinsic cell-to-cell variability may contribute to the understanding of pathological processes associated with disease development.

It is worth noting that the level of intrinsic cell-to-cell variability needs to be measured within a highly homogenous population of cells. This is because many micro-environmental perturbations and stochastic factors at the cellular level are known to change the scEV. These factors may include local cell density, cell size, shape and rate of proliferation, cell cycle, and so on (Snijder et al. 2009; McDavid et al. 2014; Kernfeld et al. 2018; Miragaia et al. 2018; Mitchell et al. 2018). To work on the cell-to-cell variability, these confounding factors have to be controlled.

Exponential scaling of scRNA-seq made it feasible to study scEV across thousands of cells (Svensson et al. 2018), and quantify scEV based on measures of statistical dispersion such as the coefficient of variation (CV)(Geiler-Samerotte et al. 2013; Mar 2019). The sheer number of cells sequenced in a "typical" droplet-based scRNA-seq experiment allows us to filter out for a sizable number of highly homogeneous cells, based on the similarity between their global transcriptional profiles. With these selected cells, we are able to test the "variation is function" hypothesis systematically. Furthermore, using established statistical methods, we are able to control for many sources of technical variation that may confound the measurement of scEV to obtain an unbiased estimate. For instance, single-molecule capture efficiency, 3' end bias due to single-cell RNA library preparation protocol, and low expression of genes are examples of known sources of technical variation (Marinov et al. 2014), which should be controlled for using statistical means.

The characterization of the impact of scEV on cell function requires the understanding of which genes show greater or less cell-to-cell variability in their expression. These feature genes may carry valuable information that can facilitate the elucidation of underlying regulatory networks (Li and You 2013). Once these genes are identified, a follow-up question is whether they are tissue- or cell type-specific—i.e., whether the same genes will be identified for different tissues or cell types. Our working hypothesis is in line with the "variation is function" hypothesis, that is, different tissues or cell types have different sets of highly variable genes (HVGs), and these

HVGs should be enriched with functions that reflect the biological functions of respective tissues or the cell types. To test this, we analyzed three scRNA-seq data sets generated for three different cell types. Each data set contains thousands of cells. For each cell type, we selected a highly homogenous population of cells, with the help of a newly developed dimensionality reduction method, called potential of heat-diffusion for affinity-based trajectory embedding (PHATE)(Moon et al. 2018). We estimated scEV among selected cells for each of these cell types and further systematically characterized functions of identified HVGs. We show that HVGs are highly specific to cell types, i.e., different cell types have different sets of HVGs; functions of HVGs precisely mirror the functions of the corresponding cell types. We explored both the level of scEV and potential mechanism behind the variability across cells, allowing us to understand a previously unexplored aspect of gene regulation in humans.

Results

Single-cell RNA sequencing and selection of highly homogenous cells

In this study, we experimented with three different human cell types, namely, lymphoblastoid cell line (LCL), lung airway epithelial cell (LAEC), and dermal fibroblast (DF). We estimated single cell expression variability (scEV) for each of these cell types, individually.

To obtain the scRNA-seq data for LCL, we cultured GM12878, an LCL strain widely used in genomic research, prepared cells using a 10X Genomics Chromium Controller, and sequenced a total of 7,045 cells (Osorio et al. 2019). This data has been deposited in the NCBI GEO database (Accession number GSE126321). For the other two cell types, LAEC and DF, we obtained the scRNA-seq data for 3,863 and 2,553 cells from the studies of (Habiel et al. 2018) and (Hagai et al. 2018), respectively (see **Data Availability**). All scRNA-seq data sets of the three cell types were produced using 10X Genomics droplet-based solution and made use of unique molecular identifiers (UMIs)(Kivioja et al. 2011).

For each cell type, we employed a data analysis procedure, a filter pipeline on scRNA-seq data, to select highly homogenous cells (**Materials and Methods**). These selected cells are a representative population of each the cell type. The main steps of the filter pipeline are depicted in **Supplementary Fig. S1**. Briefly, we first excluded mitochondrial DNA-encoded genes from the analysis. We then excluded cells in the S- or G2/M phases and only retained G1-phase cells. We also excluded cells with library size smaller than 55 percentile or greater than 99 percentile. Finally, we used PHATE to produce the embedding plot of remaining cells to inspect between-cell structure driven by heterogeneity in gene expression. PHATE is a visualization method that captures both local and global nonlinear structure in data by an information-geometry distance between data points (Moon et al. 2018). As seen from the PHATE projection (**Fig. 1A**), several "arms" of cells show the structure of the cell-to-cell relationship. Based on the observation, we manually picked one "core" cell, at the root of arms of cells, in the middle of cell cloud where the majority of cells are clustered. The core cell and 999 nearest cells around the core cell are then selected to form the final cell population, which is used for subsequent data analyses.

To examine the homogeneity of selected cells, we used t-distributed stochastic neighbor embedding (t-SNE)(van der Maaten and Hinton 2008) to position all 1,000 selected cells in the two-dimensional t-SNE space. Compared to PHATE, t-SNE is a more commonly used nonlinear visualization algorithm for revealing structures in high-dimensional data, emphasizing local neighborhood structure within the data. When running t-SNE, we experimented with a series of perplexity values to produce multiple plots for the same population of selected cells. t-SNE is known to be sensitive to hyperparameters (Becht et al. 2018). In general, when different parameter values are given, t-SNE tends to produce different cell clustering plots. But, for our selected cells, no structure is observed in any of these t-SNE embedding plots (**Fig. 1B**). The same results were obtained for the other two cell types. Thus, we confirm that cells selected with our filter pipeline are highly homogenous populations of representative cells for each cell type.

Identification of highly variable genes

Highly variable genes (HVGs) are expressed variably across homogeneous cells of the same type. For each cell type, we used the method of (Brennecke et al. 2013) to identify HVGs from scRNA-seq data of the homogeneous population of selected cells. In this method, the relationship between the squared coefficient of variation (CV^2) of genes and their average expression (μ) is considered. The relationship between log-transformed CV^2 and log-transformed μ is fitted with a Generalized Linear Model (GLM), and the expected CV^2 for a given μ is calculated with the fitted curve. The log-transformed ratio between observed CV^2 and expected CV^2 [=log(observed CV^2)- log(expected CV^2], called "residual variability", is used as the measurement of scEV. Since the expected CV^2 captures the variability originated from technical noise, the residual variability is considered to be an unbiased measure of biological variability. In total, we identified 465, 466, and 291 HVGs for LCL, LAEC, and DF, respectively (**Supplementary Tables S1-3**), after controlling for false discovery rate (FDR) at 0.01 (**Materials and Methods**). To visualize expression variability of genes, we plot CV^2 against μ, both on the logarithmic scale, for LCL (**Fig. 2A**). Each dot represents a gene; all genes together give a characteristic cloud showing the μ and CV^2 of gene expression. Genes above the GLM fitting curve, e.g., *IGKC*, *CCL3*, *LTB*, and

FTL, are more variable than expectation, whereas genes below the curve, e.g., *TMEM9B* and *RPL17*, are less variable (**Fig. 2B**).

Cell-type origin determines the function of highly variable genes

To assess the biological functions of HVGs in different cell types, we performed the enrichment analyses (**Materials and Methods**). The categories of enriched gene ontology (GO) terms and pathways of the three cell types are largely distinct and reflect the respective cell functions of each cell type (**Table 1**). Two exemplary LCL HVGs are *CCL22* and *IFI27*. Collectively, more than expected number of LCL HVGs (FDR<0.01) are involved in *cytokine-* or *interferon-signaling pathways*, and also, more generally, *innate immune system*. LAEC HVGs, including genes, *COL1A1*, *MMP1*, and *IL17C*, are more likely to be involved in the processes of *collagen formation* and *extracellular matrix organization* (FDR<0.01 for both). DF HVGs, including *KRT14*, *ACAN,* and *FLG*, are more likely to be involved in *keratinization*, *regulation of cell proliferation*, as well as *extracellular structure organization* (FDR<0.01 for all). DF HVGs also include *SFRP2*, *DPP4,* and *LSP1*, which are marker genes defining major fibroblast subpopulations in human skin (Tabib et al. 2018). Taken together, these results show different cell types have different sets of HVGs, suggesting scEV implies cell function.

If two cell types have shared function, then we expect to see the overlap in their HVG-associated functions. This indeed is the case: there are overlaps between enriched functions between the three cell types we examined here. For example, *cytokine signaling pathway* is enriched for both LCL and LAEC, and *extracellular structure organization* is enriched for both LAEC and DF. Meanwhile, across all three cell types, there are 13 shared HVGs genes: *CDC20*, *CLEC2B*, *CLIC3*, *CTSC*, *HES1*, *MT1E*, *NPW*, *SOX4*, *STMN1*, *TK1*, *TRIB3*, and *UCHL1*, showing highly diverse cellular and molecular functions.

HVGs as part of the regulatory network with high cell-type specificity

Next, we set out to test whether HVGs are co-expressed and thus tend to form co-expression networks (Mantsoki et al. 2016). We first imputed the expression matrix and then constructed the co-expressed network using the top 50 HVGs for each cell type. For LCLs, the network contains two main modules centered on *NFKBIA* and *IGHG1*, respectively (**Fig. 3A**). *NFKBIA* encodes NF-κB inhibitor that interacts with REL dimers to inhibit NF-κB/Rel complexes (Courtois et al. 2003; Lopez-Granados et al. 2008). For LAECs, two modules are centered on *IL23A*/*TNFAIP6* and *COL1A1* (**Fig. 3B**); for DF, *KRTAP2-3* and *IGFBP7* (**Fig. 3C**). Thus, functions of "hub" genes in HVG co-expression networks are closely relevant to the function of corresponding cell type. These results are another line of evidence that scEV implies cell function.

The transcription of multiple HVGs may be involved in the same underlying regulatory activities, giving rise to the co-expression network as we observed. Thus, we wondered whether scEV in several different HVGs is driven by activities of one or few common TFs. To address this question, we searched for upstream regulators of the HVGs defined by our analysis (**Materials and Methods**). We identified significant enriched TF binding motifs upstream of HVGs, four for LCL and five for LAEC (**Supplementary Table S4**). No significantly enriched motif was identified for DF. The known motifs of LCL HVGs include that of NF-κB subunit gene, *RELA*, and that of *BACH2* (**Fig. 3A**). The known motifs of LAEC HVGs include TATA box and that of *CEBPB* (**Fig. 3B**).

To further explore the involvement of HVGs in cell type-specific regulatory network, we focused on LCL HVGs in a well-studied gene regulatory network that orchestrates B cell fate dynamics (Sciammas et al. 2011; Nutt et al. 2015; Roy et al. 2019). This known regulatory network involves eight genes, including three LCL HVGs: *PRDM1* (or Blimp-1), *AICDA* (or AID), and *IRF4*, two key regulatory genes with binding motifs enriched in targeting LCL HVGs (see above): *RELA* and *BACH2*, and three other key regulators: *BCL6*, *PAX5*, and *REL* (cRel)(**Fig. 4A**). We examined the inter-relationship between across-cell expressions of three LCL HVGs (**Fig. 4B**). The scatter plot shows that the directionality of the correlation between *AICDA* and *IRF4* depends on the expression level of *PRDM1*. Among cells with relatively low expression of *PRDM1*, expressions of *AICDA* and *IRF4* are negatively correlated. Whereas, among cells in which *PRDM1* is highly expressed, expressions of *AICDA* and *IRF4* are positively correlated. This nonlinear relationship between expressions of HVGs suggests they are embedded in a tightly regulated expression network. Thus, we examined the all-by-all correlation between expressions of all eight genes in this regulatory network using the imputed data of the homogenous LCLs (**Fig. 4C**). By comparing the sign of correlation coefficient of each pair of genes with the regulatory directionality of the gene pair in the model network, we found that the correlation matrix can be used to correctly recover 16 out of 18 direct regulatory relationships. The result suggests that, even in this highly homogenous population of LCLs, cells retain gene regulatory network activities that orchestrate cell fate dynamics as in their original B cells.

Single cell expression variability is more similar between genetically related samples than unrelated samples

Given that scEV is important for cell function, we thought the level of scEV may be genetically determined. If true, then we expect that the similarity in scEV between cell lines derived from two genetically related individuals is higher than that between cell lines derived from two unrelated individuals. To test this, we performed the scRNA-seq with another LCL—GM18502, derived from a donor of African ancestry, unrelated to GM12878. We processed GM18502 along with GM12878 in the same batch (**Materials and Methods**), along with a technical replicate sample made from a 1:1 mixture of the two (Osorio et al. 2019). For comparison, we also obtained scRNA-seq data from the study of (Zhang et al. 2019) for another LCL GM12981. The donor of GM12891 is the father of GM12878. We estimated the scEV for these two additional scRNA-seq data sets: one from GM18502 (unrelated) and the other from GM12891 (father), using the same procedure applied to GM12878. To measure the correlation between scEV of different samples, we used both the Spearman correlation coefficient (SCC) and Pearson correlation coefficient (PCC). Across genes, the correlation between residual variability estimated from GM12878 and that from GM12891 (daughter-father) is ρ=0.92 (SCC) or r=0.94 (PCC)(**Supplementary Fig. S3**). That is to say, 85% (=r^2) of the variance in scEV across genes of a daughter can be explained by that of a father. In contrast, only 77% of the variance can be explained by that of an unrelated individual—the correlation between GM12878 and GM18502 is ρ=0.87 (SCC) or r=0.89 (PCC)(**Supplementary Fig. S3**).

Note that, the similarity between these two related samples, GM12878 and GM12891 (daughter and father), might have been underestimated. This is due to the gender difference between the two samples was not taken into account. Furthermore, the two scRNA-seq data sets of them were produced in different batches: GM12878 by us in this study and GM12891 by (Zhang et al. 2019). The batch effect could also influence the daughter-father correlation downward. Nevertheless, we still observed a stronger correlation between the two related samples compared to that between the two unrelated samples. These results suggest that scEV is likely to be highly heritable.

When the correlation tests were performed across cell types, much weaker correlations were observed: the correlation between LCL and LAEC is 0.60 (SCC) or 0.65 (PCC), and that between LCL and DF is 0.57 (SCC) or 0.70 (PCC).

Single cell expression variability is positively correlated with between-individual expression variability

Next, we examined the relationship between scEV and inter-individual expression variability. We distinguish between the two different types of variabilities at different organizational levels. Specifically, the former is cell-to-cell variability in a population of cells, and the latter is inter-individual variability at the human population level. We again focused on LCLs, for which population-scale gene expression data are available from the Geuvadis RNA-seq project of 1,000 Genomes samples. The bulk RNA-seq data was downloaded as normalized expression matrix of FPKM values. We retained data for all LCLs of European ancestry (CEU)(Lappalainen et al. 2013). With the residual variability estimated from scRNA-seq of GM12878 and that estimated from the CEU population, we tested the correlation between the two estimates across genes. When the test was conducted with all genes (n=8,424), we obtained a significant but weak positive correlation (SCC, $\rho = 0.19$, $p = 1.2\times10^{-9}$). We wondered whether this positive correlation was driven by subsets of genes. To identify these gene sets, we conducted the correlation tests for the GO-defined gene sets one by one. Across all gene sets tested, the average SCC for gene sets defined by GO biological process (BP) and molecular function (MF) terms are on average ρ=0.28 and ρ=0.23, respectively. Strikingly, we found a small number of gene sets that produced SCC much higher than averages. The functions of these gene sets include *B-cell activation involved in immune response* (GO: 0002322), cytokine receptor activity (GO:0004896), *cellular response to drug* (GO: 0035690) and *regulation of tyrosine phosphorylation of stat protein* (GO: 0042509)(**Fig. 5**), as well as *leukocyte chemotaxis* (GO: 0030595) and *phospholipase activity* (GO: 0004620)(for more examples, see **Supplementary Fig. S4**). Thus, for these gene sets, scEV may contribute to the establishment of between-individual expression variability.

No enriched functions associated with HVGs identified in human induced pluripotent stem cells (iPSCs)

Finally, we argued, if scEV is the indicator of cell type-specific function then scEV in undifferentiated cells should not be associated with any cellular functions. To test this, we obtained the scRNA-seq data from the study of (Nguyen et al. 2018)(see **Data Availability**). The data was generated from WTC-CRISPRi human iPSCs (Mandegar et al. 2016). Same as other cell types we examined in this study, these iPSCs were also prepared using the 10X Genomics Chromium controller. The released data contains five samples. We used the first batch (sample 1) of the data to perform the HVG detection and function enrichment tests, using the same procedure applied to other cell types. When plotting the relationship between log-transformed CV^2 and log-transformed average expression (μ), we found almost no genes showing the deviated CV2 from the regression curve (**Supplementary Fig. S5**). That is, for the majority of genes, scEV can be explained by technical noise and sampling stochasticity. Or, in other words, iPSCs lack biological variability in single cell expression. Accordingly, we found no significant GO terms or enriched pathways associated with nearly random HVGs in iPSCs. This negative result is consistent with our prediction, based on the "variation is function" hypothesis, for iPSCs, which are not expected to be associated with any cellular function found in differentiated cells.

Discussion

Single cell expression variability (or scEV) is also called gene expression noise, implying the stochastic nature of transcriptional activities in cells (Kaern et al. 2005; Raser and O'Shea 2005). Interrogating scEV data has provided insights into gene regulatory architecture (Mar et al. 2011; Chalancon et al. 2012), and manipulating the magnitude of scEV, through using noise enhancers or scEV-modulating chemicals, has been an approach to achieve drug synergies (Dar et al. 2014). Understanding the origin and functional implications of scEV has long been appreciated (Ko 1992; Fiering et al. 2000; Raj and van Oudenaarden 2008; Ecker et al. 2018).

In this study, we focused on scEV in human cells. More specifically, we wanted to characterize different expression levels of genes within a highly homogeneous population of genetically identical (or nearly isogenic) cells under the same environmental conditions. To this end, we set out to quantify scEV in highly homogeneous populations of a sizable number of viable cells. Working with cells of the same type, for example, LCL, we start by preprocessing data from thousands of cells. We found that, even though we have firstly preprocessed the data and retained only cells with similar library size and in the same cell cycle phase, it is not enough. There are still marked substructures, shown as branches of cells, in the embedding cloud of cells (**Fig. 1A**), as revealed by the new embedding algorithm (Moon et al. 2018). Retrospectively, we applied the trajectory analysis and found out that one of the longest branches contains cells with elevated expression of immunoglobulin genes (**Supplementary Fig. S5**).

Similarly, marked substructures were observed in the embedding plots of the other two cell types, LAEC and DF. Genes that were differentially expressed and drove the formation of branches of LAECs and DFs were different from those in LCL cells. Thus, there is no single or a small set of marker genes that can be used to capture cellular heterogeneity across different cell types, making the definition of populations of homogenous cells a tedious task. Our work might be the first focusing on comparing scEV in highly homogeneous cell populations across cell types.

We showed that scEV estimated from homogeneous populations of selected cells for different cell types carries information on cell type-specific function. Information on molecular functions of cells and biological processes of a given cell type can be extracted from a set of highly variable genes (HVGs), bearing significant biological meaning [see also (Dueck et al. 2015)]. HVGs detected in different cell types do not overlap and can reveal the subtle differences in cellar functions between cell types. These conclusions are reached based on our investigation of three cell types and their corresponding HVGs.

First, LCLs are usually established by in vitro infection of human peripheral blood lymphocytes with Epstein-Barr virus. The viral infection selectively immortalizes resting B cells, giving rise to an actively proliferating B cell population (Neitzel 1986). B cells genetically diversity by rearranging the immunoglobulin locus to produce diverse antibody repertories that allow the immune system to recognize foreign molecules and initiate differential immune responses (Tonegawa 1983; Papavasiliou et al. 1997; Mitchell et al. 2018). LCLs are produced through the rapid proliferation of few EBV-driven B cells from the blood cell population (Ryan et al. 2006). Thus, scRNA-seq data sets of LCLs offer a “snapshot” of highly diverse immunoglobulin rearrangement profiles in a much larger population of polyclonal B cells established in donors of these cell lines. Therefore, it is not unexpected to see quite a few immunoglobulin genes in the top list of HVGs identified in LCLs. In addition to these immunoglobulin genes, a number of other immune genes, especially C-C motif chemokine ligands (CCLs) and C-C motif chemokine receptors (CCRs), are in the list of HVGs of LCL. These genes play important roles in allowing the coordination of the activity of individual cells through intercellular communication, essential for the immune system maintains robustness (Altan-Bonnet and Mukherjee 2019). The HVG co-expression network analysis revealed the key role of the NF-κB pathway in facilitating communications between immune cells (Tay et al. 2010; Mitchell et al. 2018). More strikingly, we were able to reconstruct nearly entire NF-κB regulatory network, underlying differentiation of activated B cells and antibody-secreting cells, by using the correlation and anti-correlation relationships between expressions of HVGs and their regulatory genes.

Second, LAEC is a key cell type playing important roles in lung tissue remodeling, and pulmonary inflammatory and immune responses (Hiemstra et al. 2015). The airway epithelium, playing a critical role in conducting air to and from the alveoli, is a dynamic tissue that normally undergoes slow but constant turnover. In the event of mild to moderate injury, the airway epithelium responds vigorously to re-establish an epithelial sheet with normal structure and function. HVGs identified in LAECs, which are enriched with genes involved in collagen formation, regulation of cell proliferation, and extracellular matrix organization, accurately elucidate this aspect of functions of the airway epithelium. LAECs are also central to the defense of the lung against pathogens and particulates that are inhaled from the environment. This aspect of functions is also reflected in the enriched functionality of LAEC HVGs.

Third, DFs are responsible for generating connective tissue and play a critical role in normal wound healing (Tracy et al. 2016). DFs are also commonly used in immunological studies (Zhao et al. 2012; Ivashkiv and Donlin 2014; Hagai et al. 2018). HVGs identified in DFs again accurately reflect these primary aspects of DF functions, including extracellular matrix organization, keratinization, and regulation of signaling receptor activity. DF HVGs do have several categories of enriched functions overlap with those of LAEC, which is not unexpected, given that DF and LAEC have functional overlaps (Sacco et al. 2004).

Our results support the “variation is function” hypothesis, proposed by (Dueck et al. 2016), suggesting that the aggregate cellular function may depend on scEV. Dueck and colleagues also laid down several scenarios, including bet hedging, response distribution, fate plasticity, and so on, in which the establishment of the relationship between scEV and cell function could be attained. Our analytical framework using scRNA-seq data may be utilized in appropriate systems to test the plausibility of these different scenarios. If scEV is an accountable and credible surrogate of cell function, as we have shown in this study, then quantifying and characterizing scEV may become a first-line approach for understanding the function of cell types and tissues. Indeed, when we applied this framework to scRNA-seq data from human iPSCs, we observed no enriched gene functions and no regulatory pathways/networks associated with HVGs in iPSCs. This anti-example, showing no variation no function, further validates the “variation is function” hypothesis.

Through sequencing LCLs from three donors, we were able to compare the overall scEV across genes between related and unrelated LCL pairs. Our results suggest that scEV is a heritable trait and its relative magnitude across genes is genetically determined. In theory, the heritability of scEV can be estimated with more LCL samples from different donors of different levels of relatedness. A pairwise similarity matrix between LCLs in scEV can be regressed with the genetic relationship matrix between LCL donors, using a Haseman-Elston regression-type analysis (Haseman and Elston 1972), to quantify the heritability. The normalization between data from different LCLs (i.e., batch effect correction) can be achieved using the method of mutual nearest neighbors (Haghverdi et al. 2018), canonical correlation analysis (Butler et al. 2018) or manifold alignment (Amodio and Krishnaswamy 2018). With a population-scale scRNA-seq data set in the future, we will be able to identify mutations associated with increased scEV. At this moment, we still do not have such a resource of scRNA-seq data for samples from a sizable number of human individuals.

Nevertheless, we have shown that, across certain sets of genes, scEV is positively correlated with population-level expression variability. This correlation provides a new possibility to design single cell assays with one sample to approximate the population variability of certain genes' expression. This new method may be used to study disease-causing expression dysregulation because it has been a number of cases that increased population-level expression variability has been linked with diseases (Ho et al. 2008; Li et al. 2010; Ecker et al. 2015; Guan et al. 2016; Huang et al. 2018).

In a visionary perspective article, Pelkmans (2012) pointed out that "Embracing this cell-to-cell variability as a fact in our scientific understanding requires a paradigm shift, but it will be necessary." Indeed, scRNA-seq technologies have brought revolution to gene expression analysis. The technical development gives us a new approach beyond the capacity of traditional methods that rely on experimental measurements of population-average behavior of cells to conceive regulatory network models and signal processing pathways. More importantly, for traditional methods, by averaging information across many cells, differences among cells, which may be important in explaining mechanisms, can be lost. Given the large degree of cell-to-cell expression variability even between genetically homogeneous cells, conclusions reached as for such with traditional average-based methods may be of low-resolution, incomplete, and sometimes misleading (Tay et al. 2010; Bendall and Nolan 2012; Li and You 2013; Trapnell 2015). We have shown that scEV in highly homogeneous populations of human cells is widespread, is heritable, and implies cell function. We conclude that single cell variability and the information it contains are the key to a deepened understanding of cells and their functions. Careful assessment and characterization of cell-to-cell expression variability in relevant cell types will facilitate the study of normal cell functions as well as pathological cell processes.

Materials and Methods

LCL cell culture and scRNA-seq experiment

Two lymphoblastoid cell lines (LCLs), GM12878 (CEU) and GM18502 (YRI), were purchased from the Coriell Institute for Medical Research. They were cultured in the RPMI-1640 medium supplied with 2mM L-glutamine and 20% of non-inactivated fetal bovine serum, incubated at 37°C under 5% CO2 atmosphere. For maintenance, cells were subcultured every three days by adding fresh medium. For single cell sequencing, each cell line was subcultured with 200,000 viable cells/mL. To minimize the growth differences between those two cell lines, we plotted the growth curve by counting the viable cells which are not stained with 0.4% trypan blue every day. Both cell lines were harvested for single cell sample preparation and sequencing at day four (stationary phase) following the Sample Preparation Demonstrated Protocol and Single Cell 3' Reagent Kits v2 User Guide provided by 10X Genomics. Briefly, cells were mixed well in each flask, and 1 mL of cell suspensions from each cell line were taken out. The cells were washed three times by centrifuging, suspending and resuspending in 1X PBS with 0.04% BSA. Viable cells were then counted using an automated cell counter (Thermo Fisher Scientific, Carlsbad, CA). Cells (~5000 per cell line) were then pelleted and resuspended in the nuclease-free water based on cell suspension volume calculator table, followed by GEM (Gel Bead-In-Emulsions) generation and barcoding, the post GEM-RT cleanup, cDNA amplification, and library construction and sequencing. The experiments were conducted at the Texas A&M Institute for Genome Sciences and Society. The sequencing was conducted in the North Texas Genome Center facilities using a Novaseq 6000 sequencer (Illumina, San Diego, CA). Raw reads for each cell were analyzed using CellRanger (v2.0.0, 10X Genomics) and the outputs were aligned to the human reference genome (GRCh38) to obtain the counts.

Non-LCL scRNA-seq data sets

The scRNA-seq data for lung airway epithelial cells (LAECs) was downloaded from the GEO database using accession number GSE115982. The original data was generated in the study of (Habiel et al. 2018) for CCR10$^-$ and CCR10$^+$ LAECs. We used the data generated from the CCR10$^-$ cells with the sample identifier GSM3204305. The scRNA-seq data for primary dermal fibroblasts (DFs) was generated in the study of (Hagai et al. 2018). We downloaded the data for unstimulated DFs from the ArrayExpress database using accession number E-MTAB-5988. We also downloaded scRNA-seq data (GEO accession number GSE111912) generated in the study of (Zhang et al. 2019) for LCL sample GM12891. All of these data sets were produced using the 10X Genomics scRNA-seq solutions.

Selection of highly homogeneous populations of cells

We used a supervised data analysis method to select highly homogeneous cells based on the scRNA-seq expression profile of each cell. The procedure is summarized in a flowchart (**Supplementary Fig. S1**). The main steps are as follows. We used Seurat (v0.2)(Butler et al.

2018) to assign each cell into a cell cycle phase and excluded cells that are not considered to be in G1-phase. We removed genes encoded in the mitochondrial genome from the analysis. We then selected and retained cells with library size between 50 and 95 percentiles. We used PHATE (Moon et al. 2018) to generate embedding plot of all remaining cells and inspected the distributions of cells in the three-dimensional plot, and manually picked one "core" cell. Finally, an additional 999 cells that are closest to the core cell, according to the Euclidean distances between cells, were selected to form the final 1,000-cell population. This selection procedure was applied to each of the three cell types independently.

Identification of HVGs

Highly variable genes (HVG) is based on the assumption that genes with high variance relative to their mean expression are due to biological effects rather than just technical noise. We used the method proposed in (Brennecke et al. 2013), which is implemented in function `sc_hvg` of the scGEApp package (https://github.com/jamesjcai/scGEApp)(Cai 2019). This method starts by adjusting the library size and assumes that the observed mean expression ($\hat{\mu}_i$) and the observed CV² ($\widehat{w}_i$) of gene i among cells have the following relationship:

$$E(\widehat{w}_i) \approx a_1/\hat{\mu}_i + a_0$$

and

$$\frac{\widehat{w}_i}{a_1/\hat{\mu}_i \ + a_0} \sim \chi^2_{m-1}/(m-1)\,,$$

where m is the number of cells. The values of a_0 and a_1 are estimated by generalized linear regression (GLM). The residual term $\widehat{w}_i/(\ \hat{a}_1/\hat{\mu}_i \ + \hat{a}_0)$ for each gene is used to test if the observed CV² is significantly larger than the expected CV² via a chi-squared test. Multiple testing p-value adjustment was performed by controlling the false discovery rate (FDR)(Benjamini and Hochberg 1995).

Function enrichment analyses

To identify overrepresented biological functions of HVGs in different cell types, we performed the GO enrichment analysis using Enrichr (Chen et al. 2013; Kuleshov et al. 2016) and GOrilla (Eden et al. 2009). Enrichr was conducted for HVGs (FDR<0.01) against the rest of the expressed genes with respect to pathways collected in the Reactome pathway knowledgebase (Fabregat et al. 2018). GOrilla was performed with the list of genes sorted in descending order of their residual variability.

Analyses of Co-expression network and regulatory regions of HVGs

MAGIC (van Dijk et al. 2018) was used to impute the expression matrix. The co-expression networks were constructed using SBEToolbox (Konganti et al. 2013). The motif analysis of the regulatory regions associated with the HVGs was performed using the GREAT (McLean et al. 2010). Genomic coordinates for the HVG genes from the Human Reference Genome (hg19) were downloaded from the Ensembl Biomart (Smedley et al. 2009) and converted into bed format using an in-house script. Identified motifs were searched against the JASPAR database (Khan et al. 2018) to match the binding sites of corresponding TFs.

Data availability

The data sets produced in this study and computer code are available:

1. LCLs GM12878 and GM18502 scRNA-seq data in the Gene Expression Omnibus (GEO) database with accession number GSE126321: https://www.ncbi.nlm.nih.gov/geo/query/acc.cgi?acc=GSE126321
2. LCL GM12891 scRNA-seq data in the Gene Expression Omnibus (GEO) database with accession number GSE111912: https://www.ncbi.nlm.nih.gov/geo/query/acc.cgi?acc=GSE111912
3. LAEC scRNA-seq data in the Gene Expression Omnibus (GEO) database with accession number GSE115982: https://www.ncbi.nlm.nih.gov/geo/query/acc.cgi?acc=GSE115982
4. DF scRNA-seq data in ArrayExpress database with accession number E-MTAB-5988: https://www.ebi.ac.uk/arrayexpress/experiments/E-MTAB-5988
5. Human iPSC scRNA-seq data in ArrayExpress database with accession number E-MTAB-6687: https://www.ebi.ac.uk/arrayexpress/experiments/E-MTAB-6687
6. Computer codes used to analyze data: https://github.com/cailab-tamu/LCL_scRNA-seq

Tables

Table 1. Representative HVGs identified in the three cell types: LCL, LAEC, and DF, and the results of functional enrichment analyses. Genes are sorted by residual variability. The top 50 genes with the highest residual variability values are selected as representative HVGs.

Cell type	Highly variable genes (HVGs), top 50	Enriched GO terms, top 10	Enriched Reactome pathways, top 10
Lymphoblastoid Cell line (LCL)	*ANKRD37 ATF3 BIN1 BMP4 CAMP CCL22 CCL3 CCL3L3 CCL4 CCL4L2 CCR7 CD69 CD7 CD83 CDKN1A CTSC CYP1B1 DHRS9 DUSP2 FSCN1 HIST1H1C IER3 IFI27 IGHG1 IGHG3 IGHM IGKC ITM2A KCNMA1 LINC00176 LINC01588 LMNA LTA LTB MAL MIER2 MIR155HG MYC NFKBIA PMCH PRSS2 RGS1 RGS16 RGS2 RP11-291B21.2 S100A4 SFN TNFAIP2 TUBB4B WFDC2*	1. signal transduction (GO:0007165) 2. response to stimulus (GO:0050896) 3. immune response (GO:0006955) 4. response to biotic stimulus (GO:0009607) 5. immune system process (GO:0002376) 6. response to external biotic stimulus (GO:0043207) 7. response to external stimulus (GO:0009605) 8. cytokine-mediated signaling pathway (GO:0019221) 9. defense response (GO:0006952) 10. response to chemical (GO:0042221)	1. Immune System (R-HSA-168256) 2. Chemokine receptors bind chemokines (R-HSA-380108) 3. Interferon alpha/beta signaling (R-HSA-909733) 4. Cytokine Signaling in Immune system (R-HSA-1280215) 5. Interferon Signaling (R-HSA-913531) 6. Peptide ligand-binding receptors (R-HSA-375276) 7. G alpha (i) signalling events (R-HSA-418594) 8. Innate Immune System (R-HSA-168249) 9. Interferon gamma signaling (R-HSA-877300) 10. Cell Cycle (R-HSA-1640170)
Lung airway epithelial cell (LAEC)	*AMTN ANKRD1 AREG CCL2 CCL5 CCL7 COL1A1 COL1A2 COL3A1 COL6A1 COL6A3 CRCT1 CTGF CXCL5 CXCL6 FBXO32 GREM1 HAS2 IFNL1 IFNL2 IFNL3 IGFBP5 IGFL1 IL17C IL23A KRT14 KRT6B KRT81 LY6D MEG3 MMP1 MSMB OVOS2 PI3 POSTN PPBP RP11-338I21.1 S100A7 S100A8 S100A9 SERPINB2 SERPINB3 SERPINB4 SLC15A2 SPARC SUGCT SULF1 TEX26-AS1 TNFAIP6 TSLP*	1. regulation of multicellular organismal process (GO:0051239) 2. regulation of signaling receptor activity (GO:0010469) 3. response to stimulus (GO:0050896) 4. regulation of cell proliferation (GO:0042127) 5. developmental process (GO:0032502) 6. extracellular matrix organization (GO:0030198) 7. response to chemical (GO:0042221) 8. response to organic substance (GO:0010033)	1. Extracellular matrix organization (R-HSA-1474244) 2. Assembly of collagen fibrils and other multimeric structures (R-HSA-2022090) 3. Cytokine Signaling in Immune system (R-HSA-1280215) 4. Collagen formation (R-HSA-1474290) 5. Signaling by Interleukins (R-HSA-449147) 6. Chemokine receptors bind chemokines (R-HSA-380108) 7. Peptide ligand-binding receptors (R-HSA-375276) 8. Collagen biosynthesis and modifying enzymes (R-HSA-1650814)

		9. regulation of developmental process (GO:0050793) 10. regulation of response to stimulus (GO:0048583)	9. Integrin cell surface interactions (R-HSA-216083) 10. Class A/1 (Rhodopsin-like receptors) (R-HSA-373076)
Dermal fibroblast (DF)	*ACAN ACTA2 ACTC1 CEMIP CLU COMP CTSC CXCL1 DCN DKK1 FLG G0S2 GAL HIST1H4C IGFBP5 IGFBP7 IL1RL1 KCNMA1 KRT14 KRT17 KRT19 KRT34 KRT81 KRTAP1-5 KRTAP2-3 LCE1F LUM MGP MMP1 MMP3 MT1X NMB OLFM2 PCP4 PENK PGF PI16 POSTN PPP1R14A PTTG1 PTX3 RARRES2 RGCC SCG5 SERPINE2 SFRP2 SFRP4 STMN2 TFPI2 TNFRSF11B*	1. regulation of signaling receptor activity (GO:0010469) 2. developmental process (GO:0032502) 3. keratinization (GO:0031424) 4. anatomical structure development (GO:0048856) 5. regulation of cell proliferation (GO:0042127) 6. regulation of multicellular organismal process (GO:0051239) 7. extracellular matrix organization (GO:0030198) 8. extracellular structure organization (GO:0043062) 9. response to oxygen-containing compound (GO:1901700) 10. multicellular organismal process (GO:0032501)	1. Extracellular matrix organization (R-HSA-1474244) 2. Regulation of Insulin-like Growth Factor (IGF) transport and uptake by Insulin-like Growth Factor Binding Proteins (IGFBPs) (R-HSA-381426) 3. ECM proteoglycans (R-HSA-3000178) 4. Hemostasis (R-HSA-109582) 5. Platelet degranulation (R-HSA-114608) 6. Dissolution of Fibrin Clot (R-HSA-75205 7. Response to elevated platelet cytosolic Ca2+ (R-HSA-76005) 8. Negative regulation of TCF-dependent signaling by WNT ligand antagonists (R-HSA-3772470) 9. GPCR ligand binding (R-HSA-500792) 10. Peptide ligand-binding receptors (R-HSA-375276)

Figure legends

Fig. 1. Selection of a highly homogenous cell population for variability analysis. (**A**) Three-dimensional PHATE embedding plot for G1-phase cells of GM12878. Each point represents a single cell in the three-dimensional space. The red circle indicates the approximate positions of 1,000 selected cells. (**B**) Embedding plots generated for the 1,000 selected cells with t-SNE algorithm with a series of perplexity values.

Fig. 2. Identification of highly variable genes (HVGs). (**A**) The relationship between CV^2 and mean expression of genes in LCL GM12878. The red line shows the trend for the GLM fit curve between CV^2 and mean expression and used to identify HVGs. For each gene, the residual variability is calculated as the difference between observed CV^2 and expected CV^2 from the fitted curve. (**B**) Expression profiles of selected HVGs and lowly variable genes across cells. Cells are unsorted and remain a random order. Each vertical line is a cell and the height of line indicates the level of gene expression (UMI counts) in the cell.

Fig. 3. Co-expression networks of top HVGs. (**A**) Co-expression network between most-variable HVGs of LCL and two enriched binding motifs identified in these HVGs. (B) and (C) are for LAEC and DF, respectively.

Fig. 4. Gene regulatory network and correlation matrix of LCL HVGs. (**A**) NF-κB regulatory network model for activated B cell (ABC)-antibody secreting cell (ASC) differentiation, modified from (Roy et al. 2019). Bold font indicates HVGs; asterisk indicates the upstream TFs targeting HVGs; solid line dashed line indicates the regulatory relationship supported by the correlation between two corresponding genes, and the dashed line indicates regulatory relationship not supported by the expression correlation between genes. (**B**) Scatter plot of cells, showing the correlation between expression levels of three HVGs: *IRF4*, *AICDA* (AID) and *PRDM1* (Blimp-1). The color bar indicates the expression level of *PRDM1* (Blimp-1). (**C**) Correlation matrix between expression levels of eight genes involved in the model. Red boxes indicate that the direction of correlation between two genes is consistent with the direction of the relationship between the two in the regulatory model. Green boxes indicate inconsistency, while black boxes indicate no direct relationship according to the model. P-value in red indicated high significance ($p < 0.01$ after Bonferroni correction).

Fig. 5. Correlation between scEV (i.e., residual variability estimated from LCL GM12878) and the population-level expression variability (measured in LCLs derived from unrelated individuals of European ancestry, CEU) between genes of selected gene sets. More examples can be found in **Supplementary Fig. S3**.

Supplementary figure legends

Fig. S1. Flowchart of selection of a highly homogeneous population of cells.

Fig. S2. Correlation analyses of scEV between two genetically related LCL samples and between two genetically unrelated LCL samples.

Fig. S3. Correlation between scEV and population-level expression variability across genes of functional sets.

Fig. S4. PHATE 3-D embedding plot for cells colored according to *IGLC2* expression level in cells.

Fig. S5. The relationship between CV^2 and mean expression of genes in human iPSCs.

Acknowledgements

We thank Andrew Hillhouse and Chris Blazier for help with single cell preparation and raw data processing, Michael Criscitiello and Simon Mitchell for helpful discussions, and Barbara Gastel for writing suggestions.

Author contributions

JH and JJC conceived and designed the project; DO and XY cultured the cells; DO, YZ, GL, PY, ES, JH, and JJC analyzed the data; DO and JJC wrote the manuscript. All authors reviewed the manuscript.

Conflict of interest

The authors declare no competing interests.

Funding

This study was supported by Texas A&M University T3 grant for JJC, ES, and PY. JJC was supported by NIH grant R21AI126219.

Figures

Fig. 1.

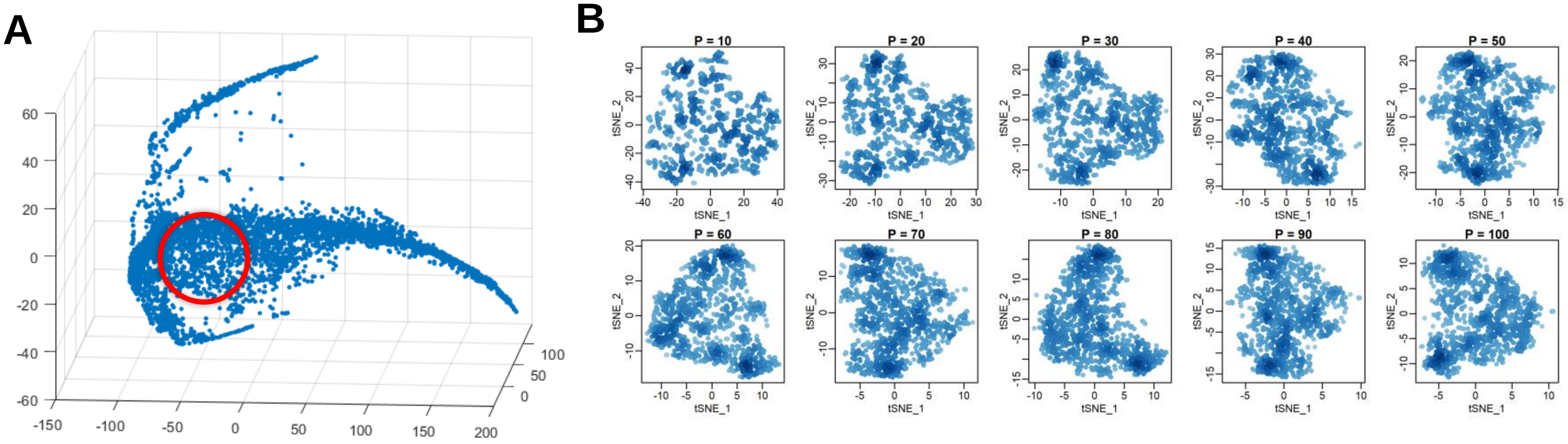

Fig. 2.

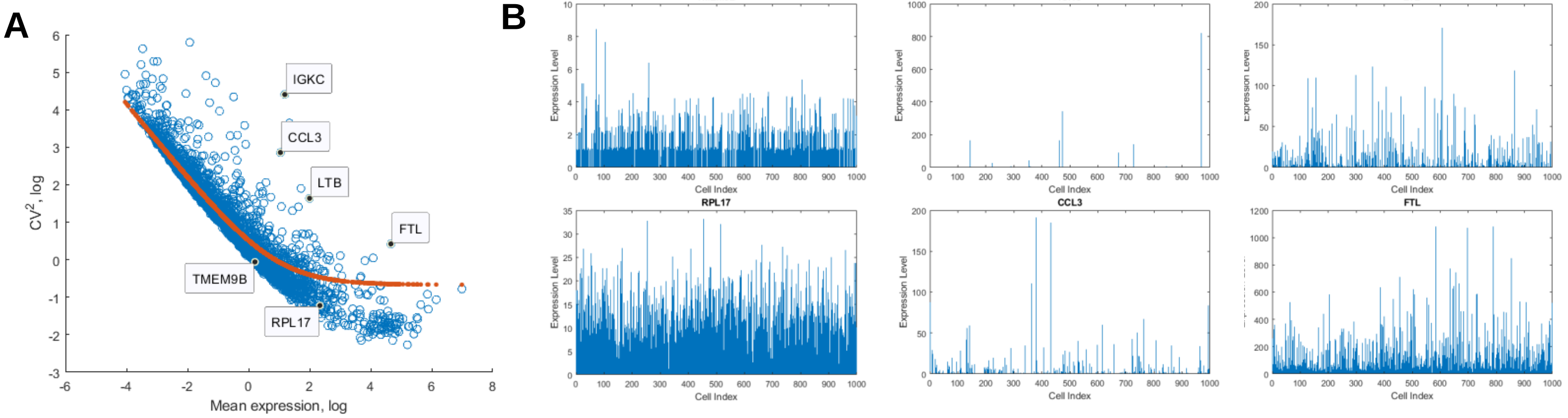
A
B
CV^2, log
Mean expression, log
IGKC
CCL3
LTB
FTL
TMEM9B
RPL17
TMEM9B
IGKC
LTB
RPL17
CCL3
FTL
Expression Level
Cell Index

Fig. 3.

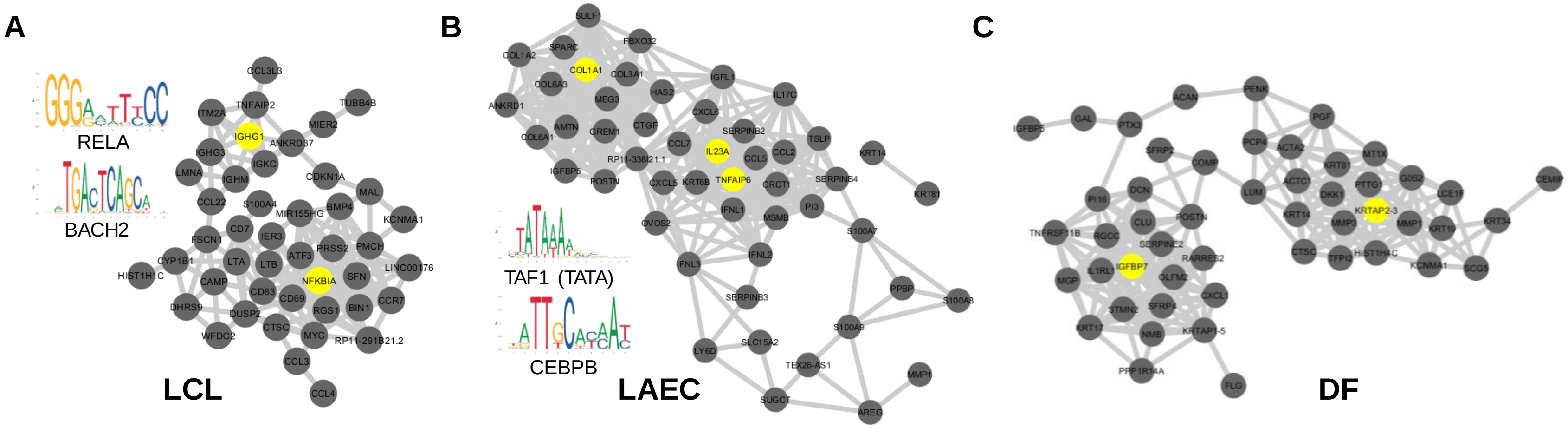
A
RELA
BACH2
CCL3L3
TNFAIP2
TUBB4B
ITM2A
IGHG1
MIER2
ANKRD37
IGHG3
IGKC
LMNA
IGHM
CDKN1A
CCL22
S100A4
MAL
MIR155HG
BMP4
KCNMA1
CD7
IER3
FSCN1
PRSS2
PMCH
ATF3
CYP1B1
LTA
LTB
LINC00176
HIST1H1C
CAMP
NFKBIA
SFN
CD83
CD69
CCR7
DHRS9
DUSP2
RGS1
BIN1
CTSC
WFDC2
MYC
RP11-291B21.2
CCL3
CCL4
LCL
B
SULF1
FBXO32
SPARC
COL1A2
COL1A1
COL3A1
COL6A3
IGFL1
HAS2
MEG3
IL17C
ANKRD1
CXCL6
AMTN
GREM1
CTGF
SERPINB2
COL6A1
TSLP
CCL7
IL23A
CCL2
KRT14
CCL5
RP11-338I21.1
IGFBP5
SERPINB4
POSTN
CXCL5
KRT6B
TNFAIP6
CRCT1
KRT81
IFNL1
PI3
MSMB
OVOS2
S100A7
TAF1 (TATA)
IFNL3
IFNL2
PPBP
S100A8
SERPINB3
S100A9
CEBPB
LY6D
SLC15A2
TEX26-AS1
LAEC
MMP1
SUGCT
AREG
C
PENK
ACAN
PGF
IGFBP5
GAL
PTX3
PCP4
ACTA2
SFRP2
MT1X
COMP
KRT81
G0S2
CEMIP
DCN
ACTC1
PTTG1
PI16
DKK1
LCE1F
LUM
POSTN
CLU
KRTAP2-3
KRT14
KRT34
TNFRSF11B
MMP3
MMP1
KRT19
RGCC
SERPINE2
CTSC
RARRES2
HIST1H4C
TFPI2
IGFBP7
KCNMA1
SCG5
IL1RL1
OLFM2
MGP
CXCL1
STMN2
SFRP4
KRT17
KRTAP1-5
NMB
PPP1R14A
FLG
DF

Fig. 4.

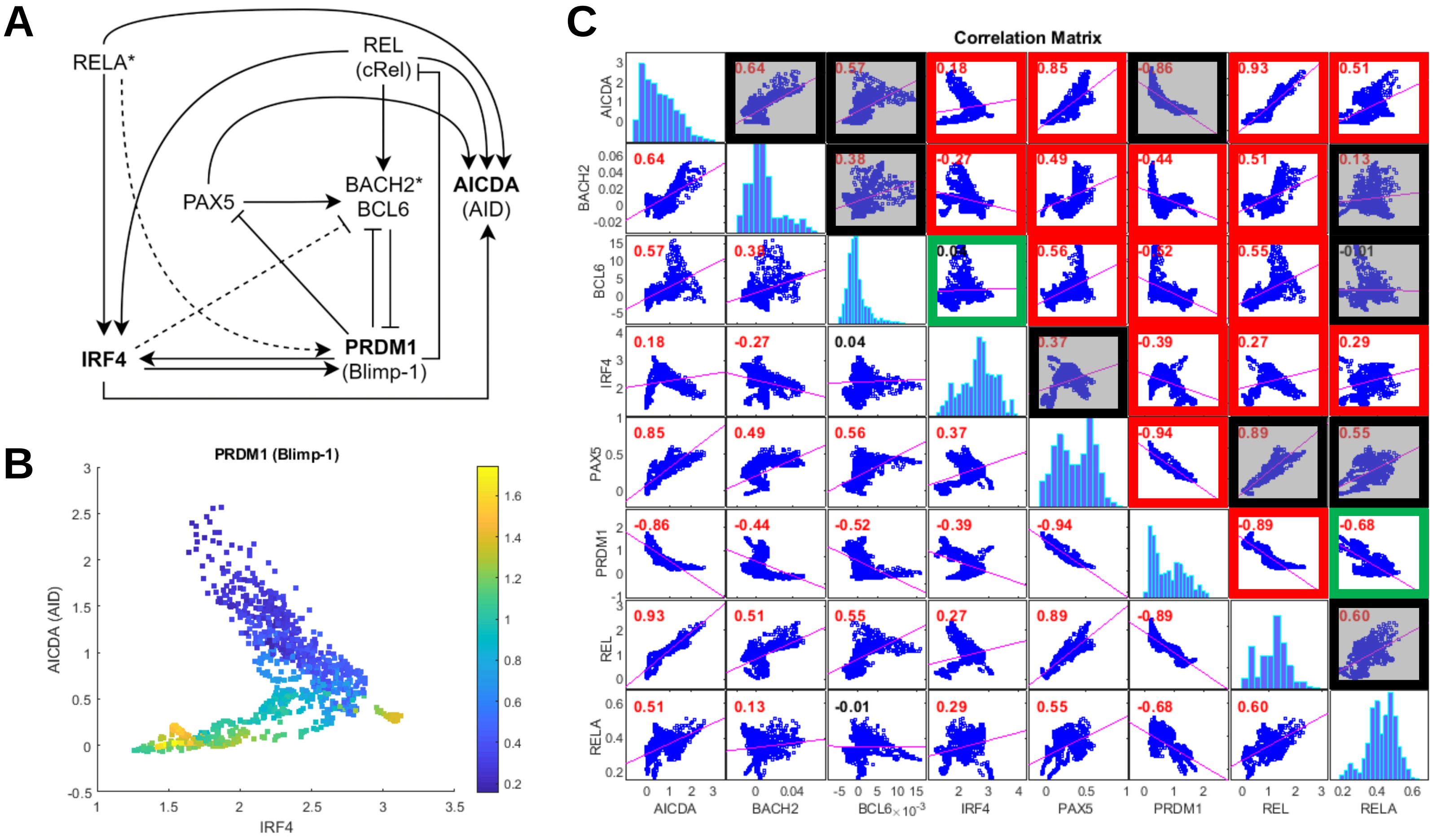
A
RELA*
REL
(cRel)
PAX5
BACH2*
BCL6
AICDA
(AID)
IRF4
PRDM1
(Blimp-1)
B
PRDM1 (Blimp-1)
AICDA (AID)
IRF4
3
2.5
2
1.5
1
0.5
0
-0.5
1
1.5
2
2.5
3
3.5
1.6
1.4
1.2
1
0.8
0.6
0.4
0.2
C
Correlation Matrix
AICDA
BACH2
BCL6
IRF4
PAX5
PRDM1
REL
RELA
0.64
0.57
0.18
0.85
-0.86
0.93
0.51
0.64
0.38
-0.27
0.49
-0.44
0.51
0.13
0.57
0.38
0.04
0.56
-0.52
0.55
-0.01
0.18
-0.27
0.04
0.37
-0.39
0.27
0.29
0.85
0.49
0.56
0.37
-0.94
0.89
0.55
-0.86
-0.44
-0.52
-0.39
-0.94
-0.89
-0.68
0.93
0.51
0.55
0.27
0.89
-0.89
0.60
0.51
0.13
-0.01
0.29
0.55
-0.68
0.60
BCL6 ×10⁻³

Fig. 5.

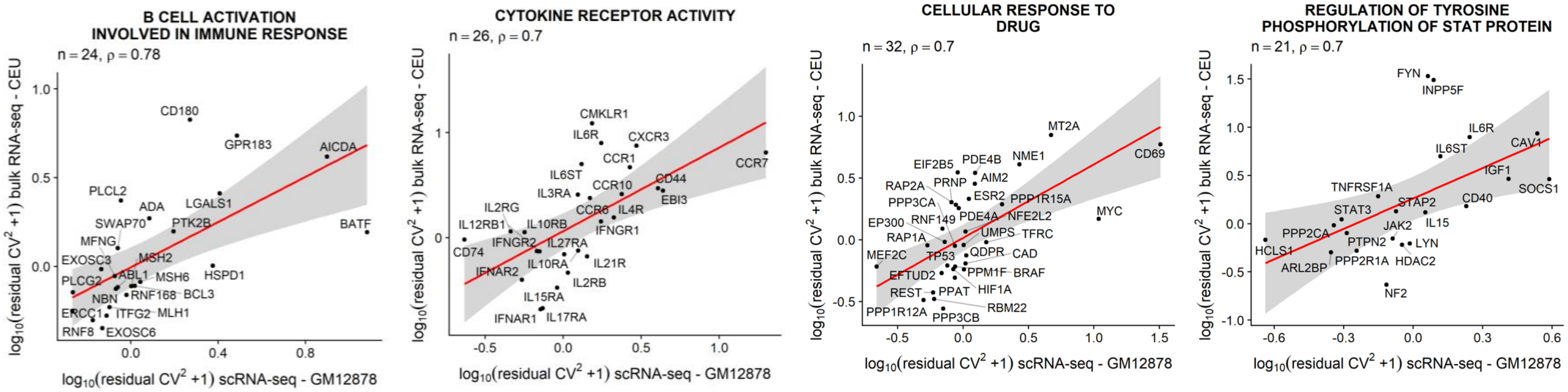

B CELL ACTIVATION INVOLVED IN IMMUNE RESPONSE

CYTOKINE RECEPTOR ACTIVITY

CELLULAR RESPONSE TO DRUG

REGULATION OF TYROSINE PHOSPHORYLATION OF STAT PROTEIN

References

Altan-Bonnet G, Mukherjee R. 2019. Cytokine-mediated communication: a quantitative appraisal of immune complexity. *Nature reviews Immunology* doi:10.1038/s41577-019-0131-x.

Amodio M, Krishnaswamy S. 2018. MAGAN: Aligning Biological Manifolds. *arXiv:180300385*.

Azizi E, Carr AJ, Plitas G, Cornish AE, Konopacki C, Prabhakaran S, Nainys J, Wu K, Kiseliovas V, Setty M et al. 2018. Single-Cell Map of Diverse Immune Phenotypes in the Breast Tumor Microenvironment. *Cell* **174**: 1293-1308 e1236.

Becht E, McInnes L, Healy J, Dutertre CA, Kwok IWH, Ng LG, Ginhoux F, Newell EW. 2018. Dimensionality reduction for visualizing single-cell data using UMAP. *Nat Biotechnol* doi:10.1038/nbt.4314.

Bendall SC, Nolan GP. 2012. From single cells to deep phenotypes in cancer. *Nat Biotechnol* **30**: 639-647.

Benjamini Y, Hochberg Y. 1995. Controlling the false discovery rate: a practical and powerful approach to multiple testing. *J Roy Statist Soc Ser B (Methodological)* **57**: 289-300.

Brennecke P, Anders S, Kim JK, Kolodziejczyk AA, Zhang X, Proserpio V, Baying B, Benes V, Teichmann SA, Marioni JC et al. 2013. Accounting for technical noise in single-cell RNA-seq experiments. *Nat Methods* **10**: 1093-1095.

Buettner F, Natarajan KN, Casale FP, Proserpio V, Scialdone A, Theis FJ, Teichmann SA, Marioni JC, Stegle O. 2015. Computational analysis of cell-to-cell heterogeneity in single-cell RNA-sequencing data reveals hidden subpopulations of cells. *Nat Biotechnol* **33**: 155-160.

Butler A, Hoffman P, Smibert P, Papalexi E, Satija R. 2018. Integrating single-cell transcriptomic data across different conditions, technologies, and species. *Nat Biotechnol* **36**: 411-420.

Cai JJ. 2019. scGEApp: a Matlab app for feature selection on single-cell RNA sequencing data. *bioRxiv* doi:10.1101/544163: 544163.

Chalancon G, Ravarani CN, Balaji S, Martinez-Arias A, Aravind L, Jothi R, Babu MM. 2012. Interplay between gene expression noise and regulatory network architecture. *Trends Genet* **28**: 221-232.

Chang HH, Hemberg M, Barahona M, Ingber DE, Huang S. 2008. Transcriptome-wide noise controls lineage choice in mammalian progenitor cells. *Nature* **453**: 544-547.

Chen EY, Tan CM, Kou Y, Duan Q, Wang Z, Meirelles GV, Clark NR, Ma'ayan A. 2013. Enrichr: interactive and collaborative HTML5 gene list enrichment analysis tool. *BMC Bioinformatics* **14**: 128.

Courtois G, Smahi A, Reichenbach J, Doffinger R, Cancrini C, Bonnet M, Puel A, Chable-Bessia C, Yamaoka S, Feinberg J et al. 2003. A hypermorphic IkappaBalpha mutation is associated with autosomal dominant anhidrotic ectodermal dysplasia and T cell immunodeficiency. *J Clin Invest* **112**: 1108-1115.

Dar RD, Hosmane NN, Arkin MR, Siliciano RF, Weinberger LS. 2014. Screening for noise in gene expression identifies drug synergies. *Science* **344**: 1392-1396.

Dueck H, Eberwine J, Kim J. 2016. Variation is function: Are single cell differences functionally important?: Testing the hypothesis that single cell variation is required for aggregate function. *Bioessays* **38**: 172-180.

Dueck H, Khaladkar M, Kim TK, Spaethling JM, Francis C, Suresh S, Fisher SA, Seale P, Beck SG, Bartfai T et al. 2015. Deep sequencing reveals cell-type-specific patterns of single-cell transcriptome variation. *Genome Biol* **16**: 122.

Ecker S, Pancaldi V, Rico D, Valencia A. 2015. Higher gene expression variability in the more aggressive subtype of chronic lymphocytic leukemia. *Genome Med* **7**: 8.

Ecker S, Pancaldi V, Valencia A, Beck S, Paul DS. 2018. Epigenetic and Transcriptional Variability Shape Phenotypic Plasticity. *Bioessays* **40**.

Eden E, Navon R, Steinfeld I, Lipson D, Yakhini Z. 2009. GOrilla: a tool for discovery and visualization of enriched GO terms in ranked gene lists. *BMC Bioinformatics* **10**: 48.

Eldar A, Elowitz MB. 2010. Functional roles for noise in genetic circuits. *Nature* **467**: 167-173.

Fabregat A, Jupe S, Matthews L, Sidiropoulos K, Gillespie M, Garapati P, Haw R, Jassal B, Korninger F, May B et al. 2018. The Reactome Pathway Knowledgebase. *Nucleic Acids Res* **46**: D649-D655.

Faure AJ, Schmiedel JM, Lehner B. 2017. Systematic Analysis of the Determinants of Gene Expression Noise in Embryonic Stem Cells. *Cell Syst* **5**: 471-484 e474.

Fiering S, Whitelaw E, Martin DI. 2000. To be or not to be active: the stochastic nature of enhancer action. *Bioessays* **22**: 381-387.

Geiler-Samerotte KA, Bauer CR, Li S, Ziv N, Gresham D, Siegal ML. 2013. The details in the distributions: why and how to study phenotypic variability. *Curr Opin Biotechnol* **24**: 752-759.

Guan J, Yang E, Yang J, Zeng Y, Ji G, Cai JJ. 2016. Exploiting aberrant mRNA expression in autism for gene discovery and diagnosis. *Hum Genet* **135**: 797-811.

Habiel DM, Espindola MS, Jones IC, Coelho AL, Stripp B, Hogaboam CM. 2018. CCR10+ epithelial cells from idiopathic pulmonary fibrosis lungs drive remodeling. *JCI Insight* **3**.

Hagai T, Chen X, Miragaia RJ, Rostom R, Gomes T, Kunowska N, Henriksson J, Park JE, Proserpio V, Donati G et al. 2018. Gene expression variability across cells and species shapes innate immunity. *Nature* **563**: 197-202.

Haghverdi L, Lun ATL, Morgan MD, Marioni JC. 2018. Batch effects in single-cell RNA-sequencing data are corrected by matching mutual nearest neighbors. *Nat Biotechnol* **36**: 421-427.

Haseman JK, Elston RC. 1972. The investigation of linkage between a quantitative trait and a marker locus. *Behav Genet* **2**: 3-19.

Hiemstra PS, McCray PB, Jr., Bals R. 2015. The innate immune function of airway epithelial cells in inflammatory lung disease. *Eur Respir J* **45**: 1150-1162.

Ho JW, Stefani M, dos Remedios CG, Charleston MA. 2008. Differential variability analysis of gene expression and its application to human diseases. *Bioinformatics* **24**: i390-398.

Huang G, Osorio Hurtado DC, Guan J, Ji G, Cai J. 2018. Overdispersed gene expression characterizes schizophrenic brains. *bioRxiv* doi:10.1101/441527.

Ivashkiv LB, Donlin LT. 2014. Regulation of type I interferon responses. *Nature reviews Immunology* **14**: 36-49.

Kaern M, Elston TC, Blake WJ, Collins JJ. 2005. Stochasticity in gene expression: from theories to phenotypes. *Nature reviews Genetics* **6**: 451-464.

Kernfeld EM, Genga RMJ, Neherin K, Magaletta ME, Xu P, Maehr R. 2018. A Single-Cell Transcriptomic Atlas of Thymus Organogenesis Resolves Cell Types and Developmental Maturation. *Immunity* **48**: 1258-1270 e1256.

Khan A, Fornes O, Stigliani A, Gheorghe M, Castro-Mondragon JA, van der Lee R, Bessy A, Cheneby J, Kulkarni SR, Tan G et al. 2018. JASPAR 2018: update of the open-access database of transcription factor binding profiles and its web framework. *Nucleic Acids Res* **46**: D1284.

Kivioja T, Vaharautio A, Karlsson K, Bonke M, Enge M, Linnarsson S, Taipale J. 2011. Counting absolute numbers of molecules using unique molecular identifiers. *Nat Methods* **9**: 72-74.

Ko MS. 1992. Induction mechanism of a single gene molecule: stochastic or deterministic? *Bioessays* **14**: 341-346.

Konganti K, Wang G, Yang E, Cai JJ. 2013. SBEToolbox: a Matlab toolbox for biological network analysis. *Evol Bioinform Online* **9**: 179-182.

Kuleshov MV, Jones MR, Rouillard AD, Fernandez NF, Duan Q, Wang Z, Koplev S, Jenkins SL, Jagodnik KM, Lachmann A et al. 2016. Enrichr: a comprehensive gene set enrichment analysis web server 2016 update. *Nucleic Acids Res* **44**: W90-97.

Kumar P, Tan Y, Cahan P. 2017. Understanding development and stem cells using single cell-based analyses of gene expression. *Development* **144**: 17-32.

Lappalainen T, Sammeth M, Friedlander MR, t Hoen PA, Monlong J, Rivas MA, Gonzalez-Porta M, Kurbatova N, Griebel T, Ferreira PG et al. 2013. Transcriptome and genome sequencing uncovers functional variation in humans. *Nature* **501**: 506-511.

Li B, You L. 2013. Predictive power of cell-to-cell variability. *Quantitative Biology* **1**: 131-139.

Li J, Liu Y, Kim T, Min R, Zhang Z. 2010. Gene expression variability within and between human populations and implications toward disease susceptibility. *PLoS Comput Biol* **6**.

Lopez-Granados E, Keenan JE, Kinney MC, Leo H, Jain N, Ma CA, Quinones R, Gelfand EW, Jain A. 2008. A novel mutation in NFKBIA/IKBA results in a degradation-resistant N-truncated protein and is associated with ectodermal dysplasia with immunodeficiency. *Hum Mutat* **29**: 861-868.

Mandegar MA, Huebsch N, Frolov EB, Shin E, Truong A, Olvera MP, Chan AH, Miyaoka Y, Holmes K, Spencer CI et al. 2016. CRISPR Interference Efficiently Induces Specific and Reversible Gene Silencing in Human iPSCs. *Cell Stem Cell* **18**: 541-553.

Mantsoki A, Devailly G, Joshi A. 2016. Gene expression variability in mammalian embryonic stem cells using single cell RNA-seq data. *Comput Biol Chem* **63**: 52-61.

Mar JC. 2019. The rise of the distributions: why non-normality is important for understanding the transcriptome and beyond. *Biophys Rev* **11**: 89-94.

Mar JC, Matigian NA, Mackay-Sim A, Mellick GD, Sue CM, Silburn PA, McGrath JJ, Quackenbush J, Wells CA. 2011. Variance of gene expression identifies altered network constraints in neurological disease. *PLoS genetics* **7**: e1002207.

Marinov GK, Williams BA, McCue K, Schroth GP, Gertz J, Myers RM, Wold BJ. 2014. From single-cell to cell-pool transcriptomes: stochasticity in gene expression and RNA splicing. *Genome Res* **24**: 496-510.

Martinez-Jimenez CP, Eling N, Chen HC, Vallejos CA, Kolodziejczyk AA, Connor F, Stojic L, Rayner TF, Stubbington MJT, Teichmann SA et al. 2017. Aging increases cell-to-cell transcriptional variability upon immune stimulation. *Science* **355**: 1433-1436.

McDavid A, Dennis L, Danaher P, Finak G, Krouse M, Wang A, Webster P, Beechem J, Gottardo R. 2014. Modeling bi-modality improves characterization of cell cycle on gene expression in single cells. *PLoS Comput Biol* **10**: e1003696.

McLean CY, Bristor D, Hiller M, Clarke SL, Schaar BT, Lowe CB, Wenger AM, Bejerano G. 2010. GREAT improves functional interpretation of cis-regulatory regions. *Nat Biotechnol* **28**: 495-501.

Miragaia RJ, Zhang X, Gomes T, Svensson V, Ilicic T, Henriksson J, Kar G, Lonnberg T. 2018. Single-cell RNA-sequencing resolves self-antigen expression during mTEC development. *Sci Rep* **8**: 685.

Mitchell S, Roy K, Zangle TA, Hoffmann A. 2018. Nongenetic origins of cell-to-cell variability in B lymphocyte proliferation. *Proc Natl Acad Sci U S A* **115**: E2888-E2897.

Moon KR, van Dijk D, Wang Z, Gigante S, Burkhardt D, Chen W, van den Elzen A, Hirn MJ, Coifman RR, Ivanova NB et al. 2018. Visualizing Transitions and Structure for Biological Data Exploration. doi:10.1101/120378 %J bioRxiv: 120378.

Neitzel H. 1986. A routine method for the establishment of permanent growing lymphoblastoid cell lines. *Hum Genet* **73**: 320-326.

Nguyen QH, Lukowski SW, Chiu HS, Senabouth A, Bruxner TJC, Christ AN, Palpant NJ, Powell JE. 2018. Single-cell RNA-seq of human induced pluripotent stem cells reveals cellular heterogeneity and cell state transitions between subpopulations. *Genome Res* **28**: 1053-1066.

Nutt SL, Hodgkin PD, Tarlinton DM, Corcoran LM. 2015. The generation of antibody-secreting plasma cells. *Nature reviews Immunology* **15**: 160-171.

Osorio D, Yu X, Yu P, Serpedin E, Cai JJ. 2019. Single-cell RNA sequencing of a European and an African lymphoblastoid cell line. *bioRxiv* doi:10.1101/548115: 548115.

Papavasiliou F, Casellas R, Suh H, Qin XF, Besmer E, Pelanda R, Nemazee D, Rajewsky K, Nussenzweig MC. 1997. V(D)J recombination in mature B cells: a mechanism for altering antibody responses. *Science* **278**: 298-301.

Pelkmans L. 2012. Cell Biology. Using cell-to-cell variability--a new era in molecular biology. *Science* **336**: 425-426.

Raj A, Rifkin SA, Andersen E, van Oudenaarden A. 2010. Variability in gene expression underlies incomplete penetrance. *Nature* **463**: 913-918.

Raj A, van Oudenaarden A. 2008. Nature, nurture, or chance: stochastic gene expression and its consequences. *Cell* **135**: 216-226.

Raser JM, O'Shea EK. 2005. Noise in gene expression: origins, consequences, and control. *Science* **309**: 2010-2013.

Roy K, Mitchell S, Liu Y, Ohta S, Lin YS, Metzig MO, Nutt SL, Hoffmann A. 2019. A Regulatory Circuit Controlling the Dynamics of NFkappaB cRel Transitions B Cells from Proliferation to Plasma Cell Differentiation. *Immunity* **50**: 616-628 e616.

Ryan JL, Kaufmann WK, Raab-Traub N, Oglesbee SE, Carey LA, Gulley ML. 2006. Clonal evolution of lymphoblastoid cell lines. *Lab Invest* **86**: 1193-1200.

Sacco O, Silvestri M, Sabatini F, Sale R, Defilippi AC, Rossi GA. 2004. Epithelial cells and fibroblasts: structural repair and remodelling in the airways. *Paediatr Respir Rev* **5 Suppl A**: S35-40.

Sciammas R, Li Y, Warmflash A, Song Y, Dinner AR, Singh H. 2011. An incoherent regulatory network architecture that orchestrates B cell diversification in response to antigen signaling. *Mol Syst Biol* **7**: 495.

Segerstolpe A, Palasantza A, Eliasson P, Andersson EM, Andreasson AC, Sun X, Picelli S, Sabirsh A, Clausen M, Bjursell MK et al. 2016. Single-Cell Transcriptome Profiling of Human Pancreatic Islets in Health and Type 2 Diabetes. *Cell Metab* **24**: 593-607.

Smedley D, Haider S, Ballester B, Holland R, London D, Thorisson G, Kasprzyk A. 2009. BioMart--biological queries made easy. *BMC genomics* **10**: 22.

Snijder B, Sacher R, Ramo P, Damm EM, Liberali P, Pelkmans L. 2009. Population context determines cell-to-cell variability in endocytosis and virus infection. *Nature* **461**: 520-523.

Svensson V, Vento-Tormo R, Teichmann SA. 2018. Exponential scaling of single-cell RNA-seq in the past decade. *Nat Protoc* **13**: 599-604.

Tabib T, Morse C, Wang T, Chen W, Lafyatis R. 2018. SFRP2/DPP4 and FMO1/LSP1 Define Major Fibroblast Populations in Human Skin. *J Invest Dermatol* **138**: 802-810.

Tay S, Hughey JJ, Lee TK, Lipniacki T, Quake SR, Covert MW. 2010. Single-cell NF-kappaB dynamics reveal digital activation and analogue information processing. *Nature* **466**: 267-271.

Tonegawa S. 1983. Somatic generation of antibody diversity. *Nature* **302**: 575-581.

Tracy LE, Minasian RA, Caterson EJ. 2016. Extracellular Matrix and Dermal Fibroblast Function in the Healing Wound. *Adv Wound Care (New Rochelle)* **5**: 119-136.

Trapnell C. 2015. Defining cell types and states with single-cell genomics. *Genome Res* **25**: 1491-1498.

van der Maaten L, Hinton G. 2008. Visualizing Data using t-SNE. *J Machin Learn Res* **9**: 2579-2605.

van Dijk D, Sharma R, Nainys J, Yim K, Kathail P, Carr AJ, Burdziak C, Moon KR, Chaffer CL, Pattabiraman D et al. 2018. Recovering Gene Interactions from Single-Cell Data Using Data Diffusion. *Cell* **174**: 716-729 e727.

Wernet MF, Mazzoni EO, Celik A, Duncan DM, Duncan I, Desplan C. 2006. Stochastic spineless expression creates the retinal mosaic for colour vision. *Nature* **440**: 174-180.

Wiley CD, Flynn JM, Morrissey C, Lebofsky R, Shuga J, Dong X, Unger MA, Vijg J, Melov S, Campisi J. 2017. Analysis of individual cells identifies cell-to-cell variability following induction of cellular senescence. *Aging Cell* **16**: 1043-1050.

Zhang X, Li T, Liu F, Chen Y, Yao J, Li Z, Huang Y, Wang J. 2019. Comparative Analysis of Droplet-Based Ultra-High-Throughput Single-Cell RNA-Seq Systems. *Mol Cell* **73**: 130-142 e135.

Zhao M, Zhang J, Phatnani H, Scheu S, Maniatis T. 2012. Stochastic expression of the interferon-beta gene. *PLoS biology* **10**: e1001249.